

# Tunable Electronics in Large-Area Atomic Layers of Boron–Nitrogen–Carbon

Baleeswaraiiah Muchharla,<sup>†</sup> Arjun Pathak,<sup>†</sup> Zheng Liu,<sup>‡</sup> Li Song,<sup>‡</sup> Thushari Jayasekera,<sup>†</sup> Swastik Kar,<sup>§</sup> Robert Vajtai,<sup>‡</sup> Luis Balicas,<sup>||</sup> Pulickel M. Ajayan,<sup>\*,‡</sup> Saikat Talapatra,<sup>\*,†</sup> and Naushad Ali<sup>†</sup>

<sup>†</sup>Department of Physics, Southern Illinois University Carbondale, Carbondale, Illinois 62901, United States

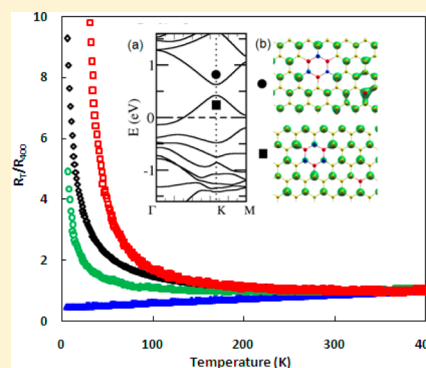
<sup>‡</sup>Department of Mechanical Engineering, Rice University, Houston, Texas 77054, United States

<sup>§</sup>Department of Physics, Northeastern University, Boston, Massachusetts 02115, United States

<sup>||</sup>National High Magnetic Field Laboratory, Florida State University, Tallahassee, Florida 32310, United States

**ABSTRACT:** We report on the low-temperature electrical transport properties of large area boron and nitrogen codoped graphene layers (BNC). The temperature dependence of resistivity ( $5\text{ K} < T < 400\text{ K}$ ) of BNC layers show semiconducting nature and display a band gap which increases with B and N content, in sharp contrast to large area graphene layers, which shows metallic behavior. Our investigations show that the amount of B dominates the semiconducting nature of the BNC layers. This experimental observations agree with the density functional theory (DFT) calculations performed on BNC structures similar in composition to the experimentally measured samples. In addition, the temperature dependence of the electrical conductivity of these samples displays two regimes: at higher temperatures, the doped samples display an Arrhenius-like temperature dependence thus indicating a well-defined band gap. At the lowest temperatures, the temperature dependence of the conductivity deviates from activated behavior and displays a conduction mechanism consistent with Mott's two-dimensional (2D) variable range hopping (2D-VRH). The ability to tune the electronic properties of thin layers of BNC by simply varying the concentration of B and N will provide a tremendous boost for obtaining materials with tunable electronic properties relevant to applications in solid state electronics.

**KEYWORDS:** Two-dimensional atomic layers, boron, nitrogen, carbon, variable range hopping, electrical transport, graphene, density functional theory calculations



The effect of impurities on the physical properties of materials with an otherwise perfectly crystalline order have intrigued scientists for decades. In this respect, the availability of 2D layered materials such as graphene<sup>1–7</sup> and the ability to introduce structural imperfections into them through impurity doping<sup>8–11</sup> (such as boron, nitrogen, etc.) has opened up possibilities for studying the consequence of disorder at the atomic level. These systems could have a unique combination of impurities including, atomically separated B and N species, as well as hexagonal boron nitride (*h*-BN) units within the graphitic C lattice. Despite its graphene-like lattice structure, *h*-BN is a wide band gap material ( $>4.5\text{ eV}$ )<sup>12</sup> due to the breakdown of its sublattice mirror symmetry. Hence, asymmetrically codoped C(B,N) with a number of B ( $n_B$ )  $\neq$  number of N ( $n_N$ ) corresponds to a unique combination of impurity doping and alloy formation within a 2D confined geometry.

The presence of *h*-BN has been shown to open up an Arrhenius-like band gap in otherwise gap-less graphene.<sup>13–15</sup> The opening of a band gap and its control in 2D systems could lead to a wide array of electronic/optoelectronic as well as sensing applications. Therefore, from the fundamental point of view the understanding of the electronic properties of 2D systems is of paramount importance, since it will give us the

ability to tune and tailor their electronic properties according to function specific needs. In this work, we present a detailed investigation of the temperature dependence of the resistivity in large-area, atomically thin layers of BNC with asymmetric codoping of B and N within the C lattice. We found that, although pure graphene shows a metallic-like temperature-dependent resistivity ( $5\text{ K} < T < 400\text{ K}$ ), the BNC layers show a semiconducting behavior<sup>16,17</sup> whose band gap increases with increasing doping levels. Density functional theory (DFT) calculations indicate that such behavior is due to the opening of a band gap resulting from either the addition of *h*-BN and/or isolated B or N within the carbon lattice. Our investigations also indicate that the tunability of the band gap of the BNC layers crucially depends on the presence of isolated B atoms within the C lattice. Further, from the temperature dependence of the resistivity of the BNC samples it is observed that, at higher temperatures ( $\sim 50\text{ K} < T < 400\text{ K}$ ), the resistivity of the doped samples show a band gap dominated Arrhenius-like temperature dependence, and below 50 K, the temperature

**Received:** February 25, 2013

**Revised:** July 14, 2013

**Published:** July 16, 2013

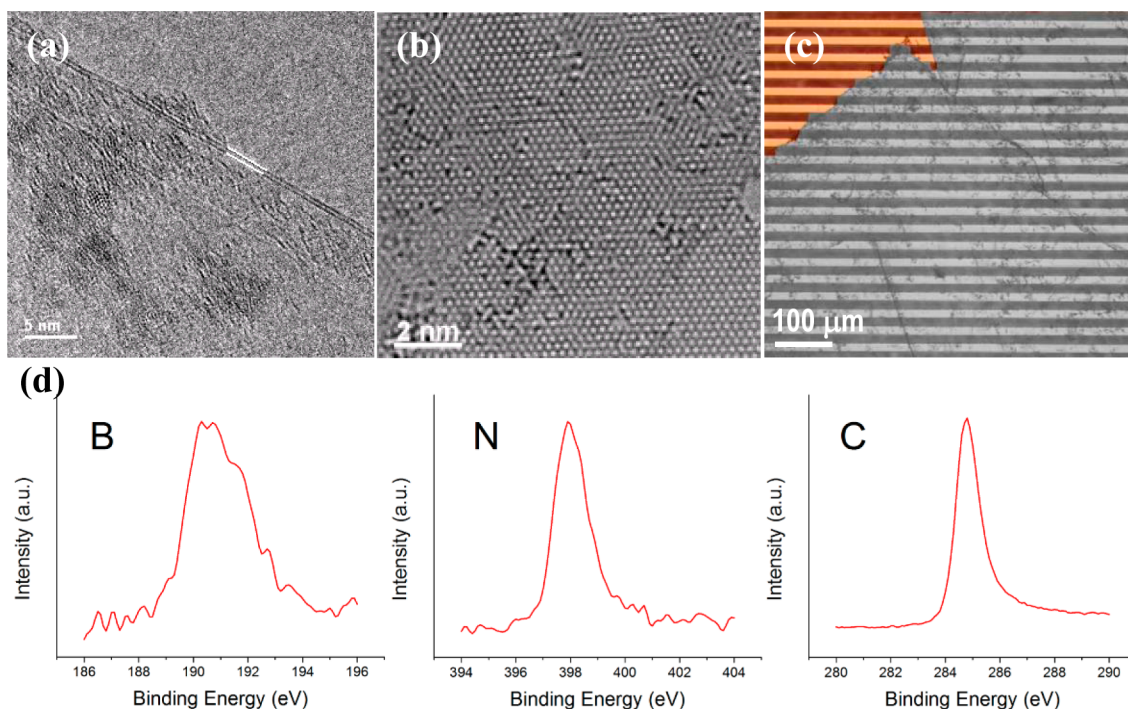


**Figure 1.** (a) TEM image of graphene layer showing two atomic layers (indicated by the two parallel white lines). (b) HRTEM of the h-BNC layer. (c) Optical image of large area BNC sample (pseudo colored) on interdigitated gold electrode with electrode separation equal to  $20 \mu\text{m}$ . The scale bar is  $\sim 100 \mu\text{m}$ . (d) Typical XPS data of h-BNC layer is shown. The peaks around  $191 \text{ eV}$  is attributed to B  $1s$ -core level, the peak at  $398.2 \text{ eV}$  is assigned to h-BN (very close to the value of  $398.4 \text{ eV}$  for N in BN), and the C  $1s$  peak located at  $284.4 \text{ eV}$  is shown.

dependence of the resistivity deviates from this activated behavior and presents evidence for a conduction mechanism that is consistent with Mott's 2D-variable range hopping (2D-VRH).

**Methods and Materials.** A chemical vapor deposition (CVD) technique was used for the synthesis of large area boron-nitride-hybridized graphene (h-BNC) described in detail elsewhere.<sup>12</sup> After the initial growth, a thin PMMA film (polymethylmethacrylate) was spun-coated onto the Cu substrates supporting the as-grown film. The underlying metal substrate was dissolved in a dilute nitric acid solution or in an iron chloride solution. Their crystallinity and composition was analyzed through transmission electron microscopy (TEM) and X-ray photoelectron spectroscopy (XPS). The films were then transferred onto interdigitated gold electrodes prepatterned onto borosilicate glass. These results are presented in Figure 1. Transport measurements on these large area films were performed in a Quantum Design SQUID magnetometer.

Computational simulations were performed using DFT as it is implemented within the Quantum Espresso package. A super cell with 128 atoms, which is equivalent to  $8 \times 8$  graphene primitive cells, was used. We used different BN concentrations and patterns to investigate their effect on the band gap. We used a  $3 \times 3 \times 1$  Monkhorst-Pack grid for the Brillouin zone integration,  $\sim 10 \text{ \AA}$  to separate the slabs, 35 Ry energy cutoff for the plane wave basis expansion, and Perdew–Burke–Ernzerhof (PBE) generalized gradient approximation (GGA) for the exchange correlation functional, and the geometries have been optimized to forces less than  $0.025 \text{ eV/\AA}$ .

**Results and Discussion.** To determine the effect of introducing B and N on the electronic properties of the C lattice, we measured the temperature dependence of the

resistivity for three large area atomic layers of BNC having the following compositions;  $\text{B}_{1.3}\text{N}_{3.4}\text{C}_{95.3}$ ,  $\text{B}_{3.1}\text{N}_{2.0}\text{C}_{94.9}$ , and  $\text{B}_{7.2}\text{N}_{3.3}\text{C}_{89.5}$  as determined by XPS. For comparison, a sample of graphene was also simultaneously measured. In Figure 2 we present the resistance (normalized to the value of the resistance at  $400 \text{ K}$ ) as a function of the temperature for all three samples. The room temperature resistances of these samples were found to be  $29.2 \Omega$  for pure graphene ( $\text{B}_{0.0}\text{N}_{0.0}\text{C}_{100}$ ),  $42.63 \Omega$  for  $\text{B}_{1.3}\text{N}_{3.4}\text{C}_{95.3}$ ,  $70.21 \Omega$  for  $\text{B}_{3.1}\text{N}_{2.0}\text{C}_{94.9}$ , and  $53.28 \Omega$  for

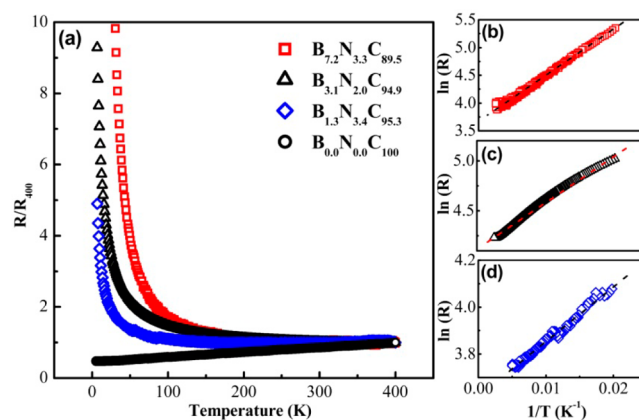


**Figure 2.** (a) Normalized resistance versus temperature curves of pure graphene and BNC samples. Resistance increased with increasing temperature for pure graphene displaying metallic behavior whereas doped samples display semiconducting behavior. (b–d)  $\ln(R)$  versus inverse temperature ( $T^{-1}$ ) for the temperature range of  $50\text{--}400 \text{ K}$ . From top to bottom data for samples of  $\text{B}_{7.2}\text{N}_{3.3}\text{C}_{89.5}$ ,  $\text{B}_{3.1}\text{N}_{2.0}\text{C}_{94.9}$ , and  $\text{B}_{1.3}\text{N}_{3.4}\text{C}_{95.3}$ , respectively, are shown. The straight lines are guide to an eye indicating linear behavior, which corresponds to the thermally activated transport mechanism in this temperature regime.

$B_{7.2}N_{3.3}C_{89.5}$ . From the data it is clear that, in the case of graphene, the resistance decreases with decreasing temperature, a manifestation of its metallic nature. Past work on graphene<sup>18,19</sup> has shown that intrinsic graphene (with  $n \approx 0$  free carriers) displays a negative temperature coefficient of its resistance (TCR), but small amounts of doping originating from the substrate or due to the device fabrication steps can render its TCR positive. Indeed, most previous investigations on graphene show<sup>20,21</sup> an inevitable p-type doping-effect due to the environment. Most likely this is the reason why our large-area samples show a positive temperature coefficient of resistance (TCR). In contrast, for all of the BNC samples studied here, we observe a nonlinear increase of the resistance with decreasing temperature (i.e., negative TCR). Overall, the nature of the variation of the resistance for the BNC layers can be broken down into two distinct temperature regimes. At higher temperatures (from 400 K to  $T^* \sim 50$  K) the resistance of the BNC samples increases slowly with decreasing temperature, but below 50 K the resistance of these samples is observed to increase sharply, which is consistent with their semiconducting nature. Furthermore, within this regime it can be clearly seen that the relative increase in resistance depends on the composition of the BNC layers, with the sharper increases observed for the samples having the higher B concentration. Such nonlinear temperature dependence of the resistivity, which is consistent with a negative TCR, has been observed for many 2D electronic systems<sup>18,22</sup> and has been analyzed at the light of various models. For example, in many semiconductors<sup>23</sup> the conduction mechanism at higher temperature follows an activated Arrhenius behavior, and the dependence of the resistance on temperature can be expressed as  $R(T) = R_0 \exp(\Delta E/k_B T)$ , where  $k_B$  is the Boltzmann constant,  $T$  is the temperature, and  $\Delta E$  is the activation energy barrier needed for the conduction process. Therefore, if the Arrhenius like activated behavior is obeyed by any given system, the plot of  $\ln(R)$  versus  $1/T$  should display a straight line. The activation energy can then be easily determined from the slope of this straight line. Figure 2b–d shows the dependence of  $\ln(R)$  as a function of  $T^{-1}$  ( $50 \text{ K} < T < 400 \text{ K}$ ) for our BNC samples. As seen, in this temperature range the data for all the three samples satisfies a linear fit, indicating that the primary conduction mechanism of the BNC layers, in this temperature regime, is Arrhenius-like. Further, it is important to note that the activation energy is strongly dependent on the composition of the BNC layers. We found that the activation energy for  $B_{1.3}N_{3.4}C_{95.3} < B_{3.1}N_{2.0}C_{94.9} < B_{7.2}N_{3.3}C_{89.5}$  (Table 1).

**Table 1. Activation Energies Calculated from the Slopes of  $\ln(R)$  versus  $T^{-1}$  Plots for *h*-BNC Samples with Different Compositions**

sample	activation energy (meV)
$B_{1.3}N_{3.4}C_{95.3}$	2.01
$B_{3.1}N_{2.0}C_{94.9}$	4.04
$B_{7.2}N_{3.3}C_{89.5}$	7.37

Therefore, it is clear from our experiments that, by decreasing the concentration of C in the BNC layers, we can drive their electrical character toward a more semiconducting nature. Since, we have used large area or millimeter sized BNC atomic layers, compositional heterogeneity is quite plausible in them. The heterogeneity in the large area BNC samples can simply arise from the following. If the B and N concentration is

very high ( $C \sim 50\%$ ), then it has been shown<sup>14</sup> that h-BN islands will form within the graphene lattice causing an inhomogeneous lattice. For example in the past,<sup>24</sup> from first-principles calculations on the basis of the density functional theory, it was established that, since BN and C are thermodynamically immiscible, separate 2D domains of h-BN in planar BNC structures are preferred. An estimated upper limit of the domain size for the film with 50 at. % C could be as big as  $\sim 42$  nm (with samples typically showing an activation gap of 18 meV). In the case of large area BNC with small amounts of BN, there are several other possibilities which will cause inhomogeneous lattice: (a) only h-BN islands as in the above case, (b) h-BN islands with BN bonds as well as (c) h-BN islands along with isolated B and/or N. This is also evident from the compositional analysis performed on the BNC films. From the compositional data obtained from our samples one can speculate an asymmetric presence of B and/or N within the C lattice. This asymmetry can lead to several configurations for B and/or the N present within the C layers. For example, apart from the h-BN islands<sup>24</sup> embedded in the C lattice, there could be isolated B or N, which would act as dopants as well as scatterers, affecting the band structure (and in turn the electrical properties) of the BNC layers. To understand the mechanism by which the doping affects the band structure of the BNC layers (which could lead to the elucidation of the temperature dependence of the resistivity seen in our experiments), we analyze through DFT calculations the electronic band gap of these structures, resulting from their atomic configurations.

A number of theoretical studies have also attempted to capture the electronic structure of the B–N–C system under various configurations, for example,  $BC_2N$ <sup>16</sup> sheets and nanoribbons,<sup>26</sup> BCN in heterographene structures,<sup>25</sup> nanotubes,<sup>17</sup> B- and N-doped carbon nanotubes,<sup>27</sup> BN–CNT heterojunctions,<sup>28</sup> and graphene nanoribbons.<sup>29</sup> Several of these studies suggest the presence of a band gap in these structures. At the same time, recent experimental investigations have clearly demonstrated the possibility of various binary and ternary atomic layers that can be built based on the BNC system.<sup>30</sup> The asymmetric presence of B and N in our BNC system implies that, in addition to the hybrid BN-graphene lattice, B and N atoms must be located at isolated configurations which are thermodynamically stable. As a result, several configurations of the BNC sheet were considered for our band structure calculations.

Table 2 summarizes all the atomic configurations we have considered in this analysis, which are also depicted in the Figure 3. The structure (a) is the pristine graphene with zero band gap at the Dirac point. While this structure is a control calculation,

**Table 2. All of the Atomic Arrangements Considered in the DFT Analysis, along with the Direct Electronic Band Gap at the Dirac Point**

system	C%	B%	N%	band gap (eV)
(a)	100	0	0	0
(b)	87.5	6.25	6.25	0.39
(c)	87.5	7.8125	4.6875	0.49
(d)	87.5	6.25	6.25	0.2735
(e)	95.3125	2.3475	2.3475	0.13
(f)	94.5313	3.125	2.34375	0.21
(g)	94.5313	2.34375	3.125	0.04

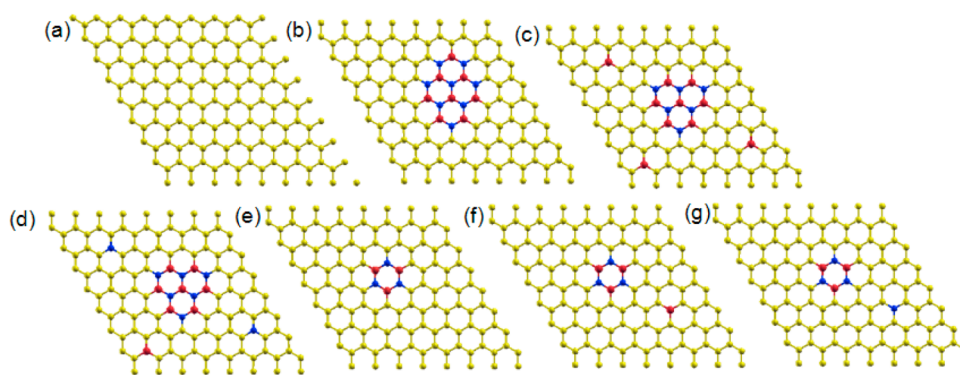


**Figure 3.** (a–g) Configurations used in the simulations. Boron = red, nitrogen = blue.

other configurations were carefully chosen to mimic the chemical composition of the samples measured in the experiment. The three experimental samples have C concentrations of 89.5%, 94.9%, and 95.3%. In our theoretical calculations, we mimic this variation by having C concentrations 87.5% (structures b,c,d), 95.3 (structure e), and 94.5 (structures f and g). Within these chosen C concentrations, the chemical composition is changed in the simulation cells to understand the role of different dopant atoms. The structures (b) and (d) have the same chemical composition, but different configurations: Structure (b) has only h-BN islands, while structure (d) contains smaller h-BN island along with isolated B and N scatterers. The structure (c) has only isolated B scatterers, no N scatterers. Our simulations clearly show that BN doping in the graphene lattice opens up a band gap at the Dirac point. A higher band gap of 0.49 eV of the structure (c) supports the fact that isolated B scatterers in the graphene honeycomb lattice dramatically break the symmetry of the  $\pi$  orbital network, thus having a higher influence in opening a band gap. A smaller amount of isolated B scatterers seem to reduce the band gap as shown in the structure (d). The simulation results on the configurations (e), (f), and (g) confirm this result. The structure (e) has a single h-BN island, structure (f) has a h-BN island along with an isolated B scatterer, and structure (g) has a h-BN island along with an isolated N scatterer. For the structures (e), (f), and (g), the electronic band gap changes from 0.13 eV, 0.21 eV, and 0.04 eV, respectively. This result clearly proves the fact that h-BN islands induce a band gap, which would be enhanced by the presence of isolated B scatterers, whereas isolated N scatterers would reduce the band gap. The higher influence of isolated B scatterers on breaking the symmetry which results in destroying the  $\pi$  orbital network is visualized by the electron orbital isosurface diagrams near the Dirac point (Figure 4). Figure 4a shows the electron band structure of the structure (f). The delocalized isosurface around the B atom in the Figure 4b visualizes the role of B-scatterers in breaking the symmetry. Figure 4d on the other hand shows the localized electron orbital isosurface around the isolated N scatterer which has a lesser effect on breaking the symmetry, resulting lower band gap opening as shown in the Figure 4c. Clearly a modulation of the Fermi level can be observed in the presence of B and N.

Several important conclusions can be drawn from these simulations results: (1) larger h-BN islands effectively destroy the  $\pi$  orbital network of  $sp^2$  hybridized graphene, inducing an electron band gap, (2) the presence of isolated B scatterers enhances this symmetry breaking, further increasing this band gap opening, and (3) the presence of N scatterers has an

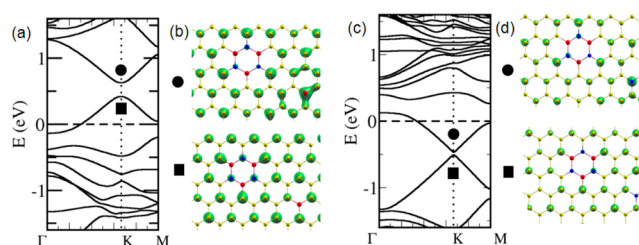


**Figure 4.** (a, c) Electronic band structures of the configurations (f) and (g), respectively, shown in Figure 3. (b, d) Electron orbital densities near the Dirac point as marked as filled circle and filled square of the configurations (f) and (g), respectively, shown in Figure 3. Red, blue, and yellow spheres show the B, N, and C, respectively. The dotted vertical line and the dashed horizontal line in the electronic band structures demarcate the K point and the Fermi level, respectively.

opposite effect from that of isolated B scatterers which reduces the band gap opening. These outcomes strongly correlate well with the trend/behavior that was observed in our experimental data; for example the introduction of BN species in C lattice introduces a band gap, and the band gap should increase with an increasing amount of B.

At low temperatures, for many disordered systems,<sup>31</sup> the conduction process deviates from activated Arrhenius behavior following a power-law relationship between the logarithm of the ohmic conductivity and the temperature. This was first proposed by Mott;<sup>32</sup> that is, at low temperatures the conduction process takes place through hopping (the so-called variable range hopping (VRH) mechanism) from occupied to unoccupied localized states present between the valence and the conduction bands. The temperature dependence of the electrical conductivity in the VRH regime is expressed as  $\sigma(T) = \sigma_0(T) \exp[-(T_0/T)^p]$ , where  $\sigma_0(T) \propto (1/T)^s$ ,  $p = 1/(d + 1)$  and  $d$  is the dimensionality of the system,  $T_0$  is the characteristic temperature, and  $s$  and  $p$  are constants. Thus, for a three-dimensional system  $p = 1/4$  while for a two-dimensional system  $p = 1/3$  manifesting a power-law<sup>33,34</sup> relationship between the logarithm of the conductivity and the temperature. In Figure 5, we plot  $\ln(R)$  as a function of  $T^{-x}$  with  $x = 1, 1/2,$  and  $1/3$ , for the h-BNC samples [(a)  $B_{1.3}N_{3.4}C_{95.3}$ , (b)  $B_{3.1}N_{2.0}C_{94.9}$ , and (c)  $B_{7.2}N_{3.3}C_{89.5}$ ], within the temperature region  $5 \text{ K} < T < 50 \text{ K}$ . Our analysis indicates that the best fits to the data are achieved for  $x = 1/3$ , indicating a 2D Mott VRH conduction mechanism in these samples.

In one of our earlier work, it was shown that, for micrometer-scale flakes of h-BNC on  $\text{SiO}_2/\text{Si}$  substrates, the BNC system

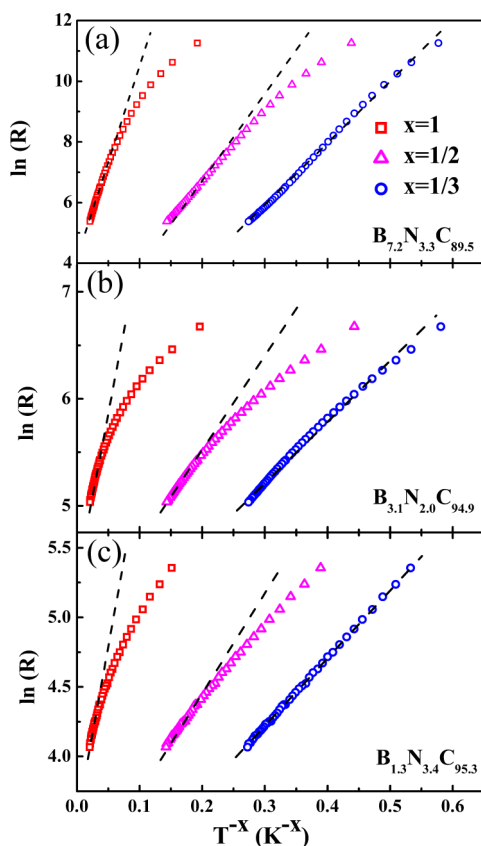


**Figure 5.** Logarithm of resistance  $\ln(R)$  of (a)  $B_{7.2}N_{3.3}C_{89.5}$ , (b)  $B_{3.1}N_{2.0}C_{94.9}$ , and (c)  $B_{1.3}N_{3.4}C_{95.3}$  samples plotted as a function of  $T^{-x}$  with  $x = 1, 1/2,$  and  $1/3$ . The dashed lines represent fits to the experimental data. It is observed that the data fit best for  $x = 1/3$ .

undergoes a striking thermodynamic insulator-to-metal transition (IMT) below  $T \sim 30$  K.<sup>14</sup> The insulating phase demonstrated an Efros–Shklovskii (E-S) type VRH temperature dependence, which is characteristic of a strongly disordered system in the absence of strong screening effects due to low carrier concentrations. The IMT was extremely robust against high magnetic fields. In contrast, we find that the high-carbon containing large area BNC samples in the present study did not show signature of such an IMT. Furthermore, the  $T$ -dependence observed here clearly indicates the absence of sufficient e–e interactions that could cause the E-S type temperature dependence. On the contrary, the 2D-Mott-type insulating behavior is clearly seen.

The significant difference between the two types of transport properties could potentially arise from a variety of reasons. First, the BNC system is known to be highly inhomogeneous as mentioned earlier, meaning that the relative concentration of the B, N, and C atoms, estimated from an “averaged” large-area sample could be quite different from the micrometer-size samples investigated in the previous report. Second, the substrate could play a key role in determining the overall screening effects experienced by the carriers confined in the 2D material. Although this effect could potentially change the type of VRH mechanism in the BNC system (from Mott to E-S type), it is hard to see any substrate-induced IMT in the BNC system. In the best likelihood, the IMT occurs in a micrometer-size BNC system, where the overall transport is at the percolation threshold of graphitic carbon within the lattice. Under this condition, the overall resistance results from a

parallel set of mechanisms, that is, a metal-like transport in the sparse graphitic network, and hopping transport between the BN islands, with the hopping transport dominating the higher temperature regime. In contrast, in the higher C-containing network (present data), the system is sufficiently above the percolation threshold of graphene and behaves like a disordered system without any strong e–e interactions.

**Conclusion.** In conclusion, we have shown the possibility of tuning the electrical properties of atomic thin large-area BNC layers. We have also provided an explanation for the variation of the electronic properties of these systems through detailed DFT calculations. The presence of larger  $h$ -BN islands effectively destroy the  $\pi$  orbital network of  $SP^2$  hybridized carbon, inducing an electronic band gap, which is increased by the presence of isolated B scatterers. While the present paper reports on the nature of the gap in large area BNC heterostructures and tries to explain, at the atomic level, which individual element B or N contributes more to this observed gap, we have observed in the past<sup>24</sup> that gaps as high as 18 meV is possible with lower C content. We note that these are transport gaps and not really band gaps, or more precisely gaps opened due to “effective band structure” due to disorder in a material, as realized for some disordered materials or random molecular alloys,<sup>35</sup> including 2D transition metal dichalcogenide alloys<sup>36,37</sup> which have some uniformity in spatial distribution of its component, and hence these materials are perhaps not yet suitable for transistors in their present form. However, if the spatial uniformity of BN in the graphene lattice can be controlled to form a near-ideal BNC alloy system, then a more systematic description of the effective band structure for these systems can be achieved. Nevertheless, there are several possible applications where 10–100 meV activation gaps could be very useful for example optical detectors and modulators in near IR to THz range. An important step in such directions will be to develop methodologies for obtaining high quality samples with homogeneous and precise compositions in a reproducible manner and overcoming possible substrate and/or environment related limitations. These results will provide a substantial knowledge base for controlling the electronic properties of 2D layered materials.

## AUTHOR INFORMATION

### Corresponding Author

\*E-mail: stalapatra@physics.siu.edu, ajayan@rice.edu.

### Notes

The authors declare no competing financial interest.

## ACKNOWLEDGMENTS

This work is supported by the U.S. Army Research Office MURI grant W911NF-11-1-0362. P.M.A., R.V., and S.T. acknowledge partial funding provided through NSF-PIRE Grant No. 0968405 for graphene-related measurements presented in the manuscript. S.T. also acknowledges partial funding provided through NSF ECCS Grant No. 0925682. S.K. received partial support from NSF ECCS Grant No. 1202376. T.J. acknowledges support from Ralph E. Powe award.

## REFERENCES

- (1) Geim, A. K.; Novoselov, K. S. The rise of graphene. *Nat. Mater.* **2007**, *6*, 183–191.
- (2) Berger, C.; Song, Z.; Li, T.; Li, X.; Ogbazghi, A. Y.; Feng, R.; Dai, Z.; Marchenkov, A. N.; Conrad, E. H.; First, P. N.; de Heer, W. A. Ultrathin epitaxial graphite: 2d electron gas properties and a route

toward graphene-based nanoelectronics. *J. Phys. Chem. B* **2004**, *108*, 19912–19916.

(3) Li, X.; Cai, W.; An, J.; Kim, S.; Nah, J.; Yang, D.; Piner, R.; Velamakanni, A.; Jung, I.; Tutuc, E.; Banerjee, S. K.; Colombo, L.; Ruoff, R. S. Large-area synthesis of high-quality and uniform graphene films on copper foils. *Science* **2009**, *324*, 1312–1314.

(4) Novoselov, K. S.; Geim, A. K.; Morozov, S. V.; Jiang, D.; Katsnelson, M. I.; Grigorieva, I. V.; Dubonos, S. V.; Firsov, A. A. Two-dimensional gas of massless Dirac fermions in grapheme. *Nature* **2005**, *438*, 197–200.

(5) Neto, C. A. H.; Guinea, F.; Peres, N. M. R.; Novoselov, K. S.; Geim, A. K. The electronic properties of graphene. *Rev. Mod. Phys.* **2009**, *81*, 109–162.

(6) Geim, A. K. Graphene: status and prospects. *Science* **2009**, *324*, 1530–1534.

(7) Geim, A. K.; MacDonald, A. H. Graphene-exploring carbon flatland. *Phys. Today* **2007**, *60* (8), 35–41.

(8) Martins, T. B.; Miwa, R. H.; da Silva, A. J. R.; Fazzio, A. Electronic and transport properties of boron-doped graphene nanoribbons. *Phys. Rev. Lett.* **2007**, *98*, 196803.

(9) Zhao, L.; He, R.; Rim, K. T.; Schiros, T.; Kim, K. S.; Zhou, H.; Gutiérrez, C.; Chockalingam, S. P.; Arguello, C. J.; Pálóvá, L.; et al. Visualizing individual nitrogen dopants in monolayer graphene. *Science* **2011**, *333*, 999–1003.

(10) Dong, J. C.; Li, H. Monoatomic layer electronics constructed by graphene and boron nitride nanoribbons. *J. Phys. Chem. C* **2012**, *116*, 17259–17267.

(11) Lherbier, A.; Blase, X.; Niquet, Y. M.; Triozon, F.; Roche, S. Charge transport in chemically doped 2d graphene. *Phys. Rev. Lett.* **2008**, *101*, 036808-1–4.

(12) Song, L.; Ci, L.; Lu, H.; Sorokin, P. B.; Jin, C.; Ni, J.; Kvashnin, A. G.; Kvashnin, D. G.; Lou, J.; Yakobson, B. I.; Ajayan, P. M. Large scale growth and characterization of atomic h-BN layers. *Nano Lett.* **2010**, *10*, 3209–3215.

(13) Pruneda, J. M. Origin of half-semimetallicity induced at interfaces of C-BN heterostructures. *Phys. Rev. B* **2010**, *81*, 161409.

(14) Song, L.; Balicas, L.; Mowbray, D. J.; Capaz, R. B.; Storr, K.; Ci, L.; Jariwala, D.; Kurth, S.; Louie, S. G.; Rubio, A.; Ajayan, P. M. Anomalous insulator-metal transition in boron nitride-graphene hybrid atomic layers. *Phys. Rev. B* **2012**, *86*, 075429.

(15) Peng, Q.; De, S. Tunable band gaps of monolayer hexagonal BNC heterostructures. *Physica E* **2012**, *44*, 1662–1666.

(16) Liu, A. Y.; Wentzcovitch, R. M.; Cohen, M. L. Atomic arrangement and electronic structure of BC<sub>2</sub>N. *Phys. Rev. B* **1989**, *39*, 1760–1765.

(17) Miyamoto, Y.; Rubio, A.; Cohen, M. L.; Louie, S. G. Chiral tubules of hexagonal BC<sub>2</sub>N. *Phys. Rev. B* **1994**, *50*, 4976–4979.

(18) Tan, Y. W.; Zhang, Y.; Stormer, H. L.; Kim, P. Temperature dependent electron transport in graphene. *Eur. Phys. J. Special Top.* **2007**, *148*, 15–18.

(19) Bolotin, K. I.; Sikes, K. J.; Hone, J.; Stormer, H. L.; Kim, P. Temperature-dependent transport in suspended graphene. *Phys. Rev. Lett.* **2008**, *101*, 096802.

(20) Novoselov, K. S.; Geim, A. K.; Morozov, S. V.; Jiang, D.; Zhang, Y.; Dubonos, S. V.; Grigorieva, I. V.; Firsov, A. A. Electric field effect in atomically thin carbon films. *Science* **2004**, *306*, 666–669.

(21) Shi, Y.; Dong, X.; Chen, P.; Wang, J.; Jong, L. Effective doping of single-layer graphene from underlying SiO<sub>2</sub> substrates. *Phys. Rev. B* **2009**, *79*, 115402.

(22) Kravchenko, S. V.; Sarachik, M. P. Metal–insulator transition in two-dimensional electron systems. *Rep. Prog. Phys.* **2004**, *67*, 1–44.

(23) Ashcroft, N. W.; Mermin, N. D. *Solid State Physics*; Thomson Brooks/Cole: Stamford, CT, 1975; pp 565–568.

(24) Ci, L.; Song, L.; Jin, C.; Jariwala, D.; Wu, D.; Li, Y.; Srivastava, A.; Wang, Z. F.; Storr, K.; Balicas, L.; Liu, F.; Ajayan, P. M. Atomic layers of hybridized boron nitride and Graphene. *Nat. Mater.* **2010**, *9*, 430–435.

(25) Yuge, K. Phase stability of boron carbon nitride in a heterographene structure- A first-principles study. *Phys. Rev. B* **2009**, *79*, 144109.

(26) Lu, P.; Zhang, Z.; Guo, W. Magnetism in armchair BC<sub>2</sub>N nanoribbons. *Appl. Phys. Lett.* **2010**, *96*, 133103-1–3.

(27) Moradiana, R.; Azadi, S. Boron and nitrogen-doped single-walled carbon nanotube. *Physica E* **2006**, *35*, 157–160.

(28) Hongxia, L.; Heming, Z.; Jiuxu, S.; Zhiyong, Z. Electronic structures of an (8, 0) boron nitride-carbon nanotube heterojunction. *J. Semiconductors* **2010**, *31*, 013001.

(29) Yu, S. S.; Zheng, W. T.; Jiang, Q. Electronic properties of nitrogen-boron-doped graphene nanoribbons with armchair edges. *IEEE Trans. Nanotechnol.* **2010**, *9*, 78–81.

(30) Song, L.; Liu, Z.; Reddy, A. L. M.; Narayanan, N. T.; Tijerina, J. T.; Peng, J.; Gao, G.; Lou, J.; Vajtai, R.; Ajayan, P. M. Binary and ternary atomic layers built from carbon, boron and nitrogen. *Adv. Mater.* **2012**, *24*, 4878–4895.

(31) Beverly, K. C.; Sampaio, J. F.; Heath, J. R. Effects of size dispersion disorder on the charge transport in self-assembled 2-D Ag nanoparticle arrays. *J. Phys. Chem. B* **2002**, *106*, 2131–2135.

(32) Mott, N. F.; Davis, E. A. *Electronic Process in Non-crystalline Materials*; Clarendon Press: Oxford, 1979; pp 34–35.

(33) Shafarman, W. N.; Koon, D. W.; Castner, T. G. dc conductivity of arsenic-doped silicon near the metal-insulator transition. *Phys. Rev. B* **1989**, *40*, 1216–1231.

(34) Withers, F.; Russo, S.; Dubois, M.; Craciun, M. F. Tuning the electronic transport properties of graphene through functionalisation with fluorine. *Nanoscale Res. Lett.* **2011**, *6*, S26 (1–11)..

(35) Popescu, V.; Zunger, A. Effective band structure of random alloys. *Phys. Rev. Lett.* **2010**, *104*, 236403.

(36) Komsa, H.; Krasheninnikov, A. V. Two-dimensional transition metal dichalcogenide alloys: stability and electronic properties. *J. Phys. Chem. Lett.* **2012**, *3*, 3652.

(37) Chen, Y.; Xi, J.; Dumcenco, D. O.; Liu, Z.; Suenaga, K.; Wang, D.; Shuai, Z.; Huang, Y.; Xie, L. Tunable Band Gap Photoluminescence from Atomically Thin Transition-Metal Dichalcogenide Alloys. *ACS Nano* **2013**, *7*, 4610.